A Closed-Form Differential Formulation
for Ultrasound Spatial Calibration

Mohammad Najafi, Narges Afsham, Purang Abolmaesumi, and Robert Rohling

University of British Columbia, Vancouver, BC, Canada
rohling@ece.ubc.ca

Abstract. *Purpose*: Calibration is essential in tracked freehand 3D ultrasound (US) to find the spatial transformation from the image coordinates to the reference coordinate system. Calibration accuracy is especially important in image-guided interventions. *Method*: We introduce a new mathematical framework that substantially improves the US calibration accuracy. It achieves this by using accurate measurements of axial differences in 1D US signals of a multi-wedge phantom, in a closed-form solution. *Results*: We report a point reconstruction accuracy of 0.3 mm using 300 independent measurements. *Conclusion*: The measured calibration errors significantly outperform the currently reported calibration accuracies.

1 Introduction

Navigation based on preoperative images usually incorporates significant registration error, especially as surgery or therapy progresses. Over the past decade, intra-operative ultrasound navigation has become a rapidly emerging technique in many procedures including neurosurgery, orthopaedic surgery and radiation therapy. Being non-invasive, relatively inexpensive, and real-time makes ultrasound (US) a valuable tool in image-guided surgeries and therapies. By attaching a position sensor to a conventional 2D US probe, 3D images can be constructed. The main challenge of this "*freehand imaging*" is to precisely locate US image pixels with respect to sensors on the transducer which is referred to as the calibration process. In this process, the objective is to determine the spatial transform between US image coordinates and the fixed coordinate system, define by the tracker on the transducer housing.

Improper or poor probe calibration has been reported as one of the major contributors to the final accuracy of ultrasound neuronavigation [1]. For example, during US-guided resection of a liver tumor, the surgeon relies on ultrasound volumes for accurate orientation with respect to the tumor. To provide more safety with respect to tumor-free resection margins and preserve vessels close to the tumor, the ultrasound system has to be calibrated accurately [2].

Over the last two decades, many approaches for calibration of 2D and 3D US have been investigated [3,4]. Examples are single wall [5], hand-eye coordination [6] and the double N-wire [7]. The most accurate calibration techniques image an artificial object, known as a phantom, with known geometrical parameters,

combining the prior knowledge of the phantom with its US images to solve for the calibration parameters. Despite numerous efforts, the best reported accuracies are in the order of 1 to 2 mm.

The limiting factor is the accurate, absolute localization of phantom features in B-mode images, which appear blurred due to the finite resolution and noise of US. Furthermore, many existing calibration methods use iterative optimization techniques to determine the calibration parameters, which are subject to sub-optimal local minima. Other factors, such as tracking accuracy and image formation errors due to speed of sound variation, refraction and finite beam width also contribute to the accuracy of calibration methods based on absolute measurements. It is worth noting that closed-form calibration from two different poses using hand-eye coordination has been proposed for measurements of relative shifts of features between images [6]. Relative measurements may have an inherent advantage, but the challenge in that method is to accurately estimate the relative 3D poses of the 2D ultrasound images.

In this paper, we propose a novel ultrasound calibration technique that alleviates many of these issues and provides substantially higher calibration accuracy. The new technique is closest to previous calibration research using wedge phantoms [6,8]. In particular, the technique uses differential measurements within the same image rather than absolute ones of phantom features in the image. Advancements in recent years on differential measurements for ultrasound motion tracking enable accurate measurements of relative phantom feature locations. This accuracy could be as high as a few microns when RF ultrasound is used [9]. The differential measurements mostly eliminate the need for absolute localization of the calibration phantom features, which has been a prominent factor in limiting the accuracy of current calibration techniques. The proposed technique also solves for variations in speed of sound and image skew. The solution to the calibration parameters also has a closed-form, which eliminates the need for an iterative optimization method.

2   Materials and Methods

The proposed calibration method is based on scanning a multi-wedge phantom that can be simply described as five different planes (Fig. 1b). The purpose of the planes is that echoes from different portions of a plane will have similar RF signatures, which enhances the ability to perform differential measurements within an image. We utilized the Field II simulation package to determine suitable angles of the planes based on image quality. In order to track the coordinate system of the phantom, four optical active markers are attached to the phantom. Also, two non-overlapping N-wires with known geometry and location relative to the planes are incorporated in the same phantom. The N-wire assembly provides an independent setup to evaluate the calibration accuracy Fig. 1a. The phantom was precisely manufactured with the Objet30 desktop 3D printer (Objet Inc., Billerica, MA, USA) to 28 μm precision and relatively low cost ($< \$200$).
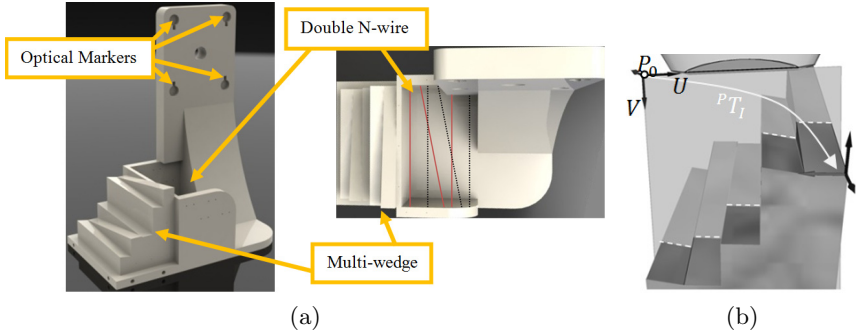
Fig. 1. (a) Multi-wedge phantom with four optical markers for tracking and an attached double N-wire phantom (b) The multi-wedge phantom comprising of five different planes. The dashed line shows the ultrasound image intersection line segments.

The calibration experimental setup consists of a SonixTOUCH ultrasound machine (Ultrasonix Medical Corporation, Richmond, BC, Canada), a L14 − 5, 10 MHz linear 2D ultrasound transducer, and an Optotrak Certus optical tracker (Northern Digital Inc, Waterloo, Ontario, Canada).

In our experiments, the coordinate systems of the phantom and the ultrasound transducer are measured by tracking the optical markers mounted on them (Fig. 2a). Therefore transformation from the phantom to the transducer coordinate can be found ($^T T_P$). The calibration goal is to find transformation from the image to the transducer coordinate ($^T T_I$). To solve that, we must calculate the image to phantom transformation ($^P T_I$).

Each plane appears as a line in the ultrasound image (dashed lines in Fig. 1b). The slope and intercept of these lines depend on the pose of the ultrasound image relative to the phantom. In fact, the goal is to find the pose of the US image ($^P T_I$) by measuring these line features in the ultrasound image. For this reason, a closed-form algorithm has been developed to estimate the calibration parameters using a single ultrasound image given the geometrical model of the phantom.

2.1   Mathematical Framework and Notations

We define the calibration phantom with the equations of five different planes. Here, we assume that the normal vector (n_i) and a point (Q_i) of each plane is known in a common coordinate system (i.e. the phantom coordinates).

The unknown transformation from the image to the phantom frame, ($^P T_I$), can be defined from two free vectors U and V and a point P_0 as follows (Fig. 2b). U is a unit vector in the direction passing through the center of array elements (lateral) and V is a unit vector in the direction of ultrasound beam (axial). These two vectors are usually assumed to be perpendicular but here we do not impose this assumption for a more general solution. P_0 is the origin of imaging plane in the phantom coordinates and is the translation vector in $^P T_I$.

2.2 Rotation Parameters

We first estimate the rotation parameters in $^{P}T_I$ by calculating vectors U, V and S_y and then, by solving for P_0 we determine the translation parameters. Each pixel (x_1, y_1) of the image can be described in the phantom coordinates as:

$$P = P_0 + S_x x_1 U + S_y y_1 V. \tag{1}$$

Considering the pixels on the line appeared in the ultrasound image from the intersection of the phantom's i^{th} plane and the ultrasound image plane, they should satisfy the plane equation for plane i (Fig. 2b):

$$[P_0 + S_x x_1 U + S_y y_1 V - Q_i] \cdot n_i = 0, \tag{2}$$

$$P_0 \cdot n_i + S_x x_1 \underbrace{U \cdot n_i}_{\alpha_i} + S_y y_1 \underbrace{V \cdot n_i}_{\beta_i} = \underbrace{Q_i^t \cdot n_i}_{d_i}, \tag{3}$$

Now assume another point (x_2, y_2) in the image that is also on the intersection line of the same phantom plane.

$$P_0 \cdot n_i + S_x x_2 U \cdot n_i + S_y y_2 V \cdot n_i = Q_i^t \cdot n_i, \tag{4}$$

Now by subtracting Eq. 4 from Eq. 3 and then dividing by S_x, we have:

$$\Delta x U \cdot n_i + K \Delta y V \cdot n_i = 0. \tag{5}$$

where $K = \frac{S_y}{S_x}$, $\Delta x = x_2 - x_1$ and $\Delta y = y_2 - y_1$. By dividing Eq. 5 by Δx and assuming $m = \frac{\Delta y}{\Delta x}$, we have:

$$U \cdot n + K m V \cdot n = 0. \tag{6}$$
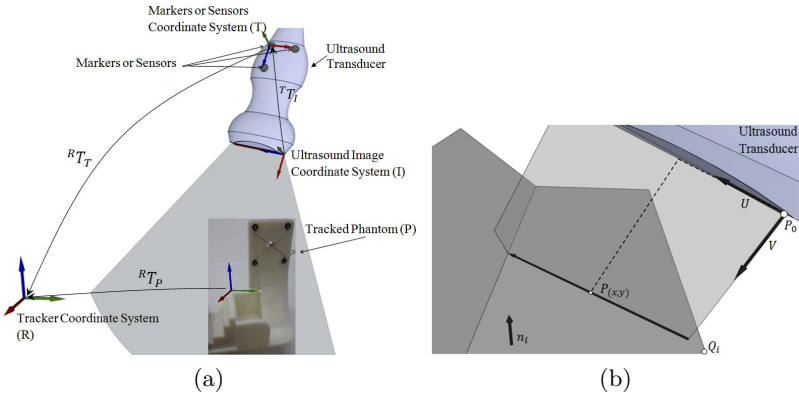
Fig. 2. (a) The coordinate system of the phantom and the ultrasound transducer. (b) Intersection of the ultrasound image and the phantom i^{th} plane .

In fact, m is the slope of the intersection line that can be measured from the ultrasound image. At least five linear equations such as Eq. 6 for five independent planes are needed to solve for the unknowns subject to the unity constraint of U and V. One can write equations in matrix form as follows:

$$N_{p\times3}U + KM_{p\times p}N_{p\times3}V = 0. \tag{7}$$

where $N = (n_1^t, n_2^t, \ldots, n_p^t)_{p\times3}$, $M = diag(m_1, m_2, \ldots, m_p)_{p\times p}$ and p is the number of planes. Eq. 7 can be re-written as below:

$$\begin{bmatrix} N_{p\times3} & MN_{p\times3} \end{bmatrix} \begin{bmatrix} U \\ KV \end{bmatrix} = 0. \tag{8}$$

In fact, Eq. 8 is a set of linear equations with the right side equal to zero. If we divide both sides by U_x and move $-n_{i_x}$ to the right (for each row i) and define new unknowns as $X = \begin{bmatrix} \frac{u_y}{u_x} & \frac{u_z}{u_x} & K\frac{v_x}{u_x} & K\frac{v_y}{u_x} & K\frac{v_z}{u_x} \end{bmatrix}^t$, we get a set of linear equations with non-zero values on the right side:

$$\begin{bmatrix} n_{1_y} & n_{1_y} & m_1 n_{1_x} & m_1 n_{1_y} & m_1 n_{1_z} \\ \vdots & \vdots & \vdots & \vdots & \vdots \\ n_{p_v} & n_{p_y} & m_p n_{p_x} & m_p n_{p_y} & m_p n_{p_z} \end{bmatrix}_{p\times5} \begin{bmatrix} \frac{u_y}{u_x} \\ \frac{u_z}{u_x} \\ K\frac{v_x}{u_x} \\ K\frac{v_y}{u_x} \\ K\frac{v_z}{u_x} \end{bmatrix}_{5\times1} = - \begin{bmatrix} n_{1_x} \\ \vdots \\ n_{p_y} \end{bmatrix}_{p\times1} \tag{9}$$

This gives a unique solution for $p = 5$ simply by solving a set of five linear equations with five unknowns (X). Then U, V and K can be uniquely found from:

$$U = \frac{[1, x_1, x_2]}{\|[1, x_1, x_2]\|}, \quad V = \frac{[x_3, x_4, x_5]}{\|[x_3, x_4, x_5]\|}, \quad K = \|[x_3, x_4, x_5]\| u_x. \tag{10}$$

This solution is the same as the Null space of Eq. 8. For $p > 5$ we can find the solution in a least-squares sense. The above derivation also explains the need for five planes. Another way of getting a non-zero value on the right side is by taking the differences of two columns on two different parallel wedges with a specified height difference. Therefore this known height difference would appear on the right side of Eq. 5. In the case of steered ultrasound beam, U and V are not orthogonal and the deviation of their crossing angle from 90° can be expressed as the skew angle. Up to this point, the rotational matrix, skew and S_y are determined from U, V and K.

2.3   Translation Parameters

In Eq. 3, d_i and S_x are known and S_y, U and V have been determined from previous step, so α_i and β_i are also known. For any arbitrary column x_i in the image, the position of the line y_i should be measured. Using Eq. 3 for at least three planes gives a set of linear equations with three unknowns (i.e. the coordinates of P_0) that is straight forward to solve. It can also be solved with more than three points in a least-squares sense to improve accuracy.
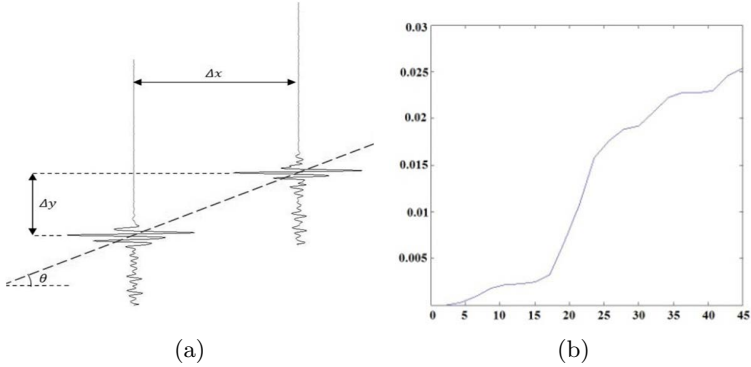
Fig. 3. (a) (Left) Slope measurement with RF cross-correlation. $\tan(\theta) = \frac{\Delta y}{\Delta x}$ (b) (Right) Slope measurement error ($\frac{Error(\Delta y)}{\Delta x}$) versus the angle between the beam and plane normal vector (φ).

2.4   Phantom Design

As mentioned, phantom design was optimized using simulated RF images from the Field II ultrasound simulation package. The goal is to find a suitable angle of each wedge so that the line segments are clear in the image and can be segmented accurately while the slopes are still large enough to achieve lowest sensitivity of the calibration results to the measurement error.

This design trade off can be better understood by explaining the RF image formation and the measurement process. Each column of an ultrasound image is formed by envelope detection of an RF echo signal. The spacing between the columns depends on the spacing of the transducer's elements, which is generally provided by the manufacturer. Axial resolution depends on the RF center frequency, the sampling rate of ultrasound machine, and speed of sound.

When imaging a flat surface with ultrasound, the RF echo pulse in each column is reflected at a specific point. All these points reside on a straight line with measurable slope (Fig. 3a). As long as the pulse shapes of at least two columns are similar, accurate slope measurement is possible by finding their axial shift with a cross correlation technique [9]. Due to the high axial resolution, a very accurate measurement can be performed. If the ultrasound beam axis is perpendicular to the surface, the shape of the RF pulses in all the columns will be the same since they all experience the same physical conditions. However, the shape of the returned echo changes slightly as the angle between the beam axis and the normal of the surface increases. This is because of the non-uniform point spread function of the ultrasound beam.

In the Field II simulation package, we modeled a plane with a number of discrete scatterers. The angle between the beam axis and the plane normal, φ, is chosen in the interval of 0 to 30 degrees and the error in the slope measurement is calculated (Fig. 3b). Results show that as the plane tilts towards higher angles with respect to the ultrasound beam, the change in the pulse shape for different

columns leads to larger errors in slope measurement. These results agree with our experimental results when imaging a flat metallic surface immersed in water in different poses. In this work, the phantom is constructed with 10° wedges as a reasonable compromise.

3   Results

3.1   Calibration Repeatability

For calibration, 15 different images of the multi-wedge phantom are acquired. All the images are processed in a semi-automatic procedure where the user verifies the suggested line segments found by a line detection algorithm and, if necessary, identifies the appropriate edge points of each line segment. Then based on the cross correlation technique, the slope of each line is calculated from pairs of RF data. Lastly, after fitting a line to each segment, the middle point (x_i) is taken and its depth (y_i) is automatically measured from the peak of the RF pulse. Although this value is an absolute measurement, with greater inherent error than differential measurements, the result (translation parameters) is not very sensitive to this measurement (investigated later in this section). To evaluate the calibration repeatability, the calibration is solved using all the images except one for all 15 possible combinations and the standard deviation is calculated (Table. 1). Similarly, the calibration is evaluated using different numbers (n_s) of images. Each time, $n_s(=2$ to $14)$ images are randomly chosen from all 15 images and the calibration is solved. The standard deviation and the average of the results over 250 iterations have been calculated and shown in Fig. 4. It shows that standard deviation of error rapidly decreases as the number of input images increases and a few number of images are sufficient to achieve very accurate results. Note that given the closed-form formulation, the order of the images is unimportant.

3.2   Calibration Accuracy

In order to evaluate the calibration results, an independent validation experiment was performed. A set of six independent wires similar to a double N-wire phantom in [7] was integrated into the phantom (Fig. 1). The position of the wires is measured by a tracked stylus. 50 different images of this N-wire phantom were then acquired from different transducer positions. Using the calculated calibration matrix, and the measurements of the poses of the transducer and the

Table 1. Standard deviation of 15 calibration results using 14 images at a time

	Rotaion (°)			Translation(mm)		
	r_x	r_y	r_z	t_x	t_y	t_z
Error Standard Deviation	0.005	0.18	0.37	0.02	0.02	0.18

Table 2. Calibration accuracy in terms of point reconstruction error (300 points)

Error	Standard deviation (mm)	Mean(mm)
x	0.22	0.25
y	0.12	0.11
$Distance$	0.23	0.29

wires from the tracker, the six intersection points of the wires with the ultrasound image were estimated in ultrasound image coordinates. These estimated points were then compared to the actual points appearing in the image. The centroid of these points were also segmented manually and the error in x and y directions and the Euclidian distance error are calculated for all points ($50 \times 6 = 300$) and shown in Table. 2.

3.3   Sensitivity to Absolute Measurement

As mentioned, skew, scale and rotation parameters are calculated using accurate differential measurements, but to find translation parameters, absolute depth (y_i) of the lines at column x_i is measured from the peak of the RF pulse.

Therefore we can assume there is an error in measurement of y_i which can be modeled as a random noise in the range of the pulse length ($0.1\ mm$). To evaluate the sensitivity of calibration translation parameters to this error, a random noise
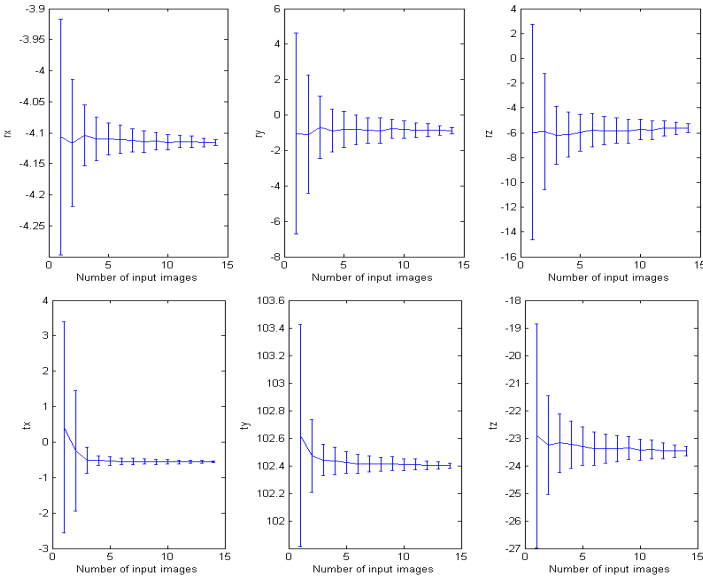
Fig. 4. Calibration results using 2 to 14 images of the phantom (top) Translation parameters (t_x, t_y, t_z) $[mm]$ (bottom) Rotation parameters $(r_x, r_y, r_z\ )$ $[deg]$

Table 3. STD of error in the translation parameters when normal noise ($\sigma = 0.1\ mm$) added to y_i

STD of error in translation parameters(mm)		
x	y	z
0.19	0.02	0.2

having a normal distribution ($\sigma = 0.1\ mm$) has been added to y_i measurements and the standard deviation of the translation parameters have been calculated (1000 iterations) and shown in Table. 3. Note that the true surface (wedge) location is not necessarily the peak of the RF pulse and is not easy to find [10], but the true surface lies within the echo, so any remaining systematic errors should be less than the pulse length.

4 Discussion and Conclusion

In this paper, a novel closed-form method is proposed for freehand $3D$ ultrasound calibration that extends upon previous calibration techniques. The method has been developed based on the specific physical properties of ultrasound imaging system. The relative shift of two RF-echo pulses hitting the same plane surface seems to be a very accurate measure to base a calibration technique. With this in mind, based on the simulations and the experiments, a multi-wedge phantom has been proposed. There is a trade-off in the design of the phantom. For a given measurement error the calibration error decreases as the surfaces in the phantom become steeper and more distanced from each other but on the other hand, the measurement error for those surfaces gets larger.

Experimental results show that a few (~ 10) images of the phantom are required for high accuracy. Also, independent accuracy evaluation of the calibration results confirms the high accuracy of the proposed method. Location of target points (N-wire intersections with the ultrasound imaging plane) has been estimated with less than 0.3 mm accuracy. This accuracy also includes the error from segmentation of the points, so calibration error is less than this total.

Although it is incorrect to compare calibration accuracy between systems with different transducers, ultrasound machines, and trackers, it is worth citing an example where 10,000 images of the double N-wire phantom gave a point reconstruction error of 0.66 mm [7]. The authors could not find previous calibration results with an accuracy of 0.3 mm.

The phantom can be enclosed in a sterile fluid-filled rubber-topped box for intra-operative use. The calibration procedure is very easy and fast by taking several images of the phantom in a fast sweep. Image processing can be performed in real-time. Therefore, calibration will take less than one minute.

Future work will extend this method to curvilinear and 3D transducers. Our initial investigations show that a new formulation based on polar coordinates requires even fewer numbers of images because many more plane orientations are available in a single image due to the non-parallel nature of the beams.

Such work will proceed on both pre- and post-scan converted data. Given the inexpensive and easy manufacturing of the phantom, this calibration method can be disseminated to a wide range of researchers by sharing CAD files and program code.We will integrate the software in the PLUS library for public use.

References

1. Lindseth, F., Lang, T., Bang, J., Nagelhus Hernes, T.A.: Accuracy evaluation of a 3D ultrasound-based neuronavigation system. Computer Aided Surgery: Official Journal of the International Society for Computer Aided Surgery 7(4), 197–222 (2002); PMID: 12454892
2. Gulati, S., Berntsen, E.M., Solheim, O., Kvistad, K.A., Hberg, A., Selbekk, T., Torp, S.H., Unsgaard, G.: Surgical resection of high-grade gliomas in eloquent regions guided by blood oxygenation level dependent functional magnetic resonance imaging, diffusion tensor tractography, and intraoperative navigated 3D ultrasound. Minimally Invasive Neurosurgery: MIN 52(1), 17–24 (2009); PMID: 19247900
3. Mercier, L., Lang, T., Lindseth, F., Collins, D.L.: A review of calibration techniques for freehand 3-D ultrasound systems. Ultrasound in Medicine & Biology 31(4), 449–471 (2005); PMID: 15831324
4. Hsu, P., Prager, R., Gee, A., Treece, G., Sensen, C., Hallgrmsson, B.: Freehand 3D ultrasound calibration: A review. Advanced Imaging in Biology and Medicine, 47–84 (2009)
5. Prager, R.W., Rohling, R.N., Gee, A.H., Berman, L.: Rapid calibration for 3-D freehand ultrasound. Ultrasound in Medicine & Biology 24(6), 855–869 (1998)
6. Boctor, E.M., Iordachita, I., Choti, M.A., Hager, G., Fichtinger, G.: Bootstrapped ultrasound calibration. Studies in Health Technology and Informatics 119, 61–66 (2006); PMID: 16404015
7. Chen, T.K., Thurston, A.D., Ellis, R.E., Abolmaesumi, P.: A Real-Time freehand ultrasound calibration system with automatic accuracy feedback and control. Ultrasound in Medicine & Biology 35(1), 79–93 (2009)
8. Afsham, N., Chan, K., Pan, L., Tang, S., Rohling, R.N.: Alignment and calibration of high frequency ultrasound (HFUS) and optical coherence tomography (OCT) 1D transducers using a dual wedge-tri step phantom. In: Proceedings of SPIE, vol. 7964, p. 796428 (March 2011)
9. Zahiri-Azar, R., Salcudean, S.E.: Motion estimation in ultrasound images using time domain cross correlation with prior estimates. IEEE Transactions on Biomedical Engineering 53(10), 1990–2000 (2006)
10. Hacihaliloglu, I., Abugharbieh, R., Hodgson, A.J., Rohling, R.N.: Bone surface localization in ultrasound using image Phase-Based features. Ultrasound in Medicine & Biology 35, 1475–1487 (2009)